Prediction of Interfacial Properties of High-Performance Polymers and Flattened CNT-Reinforced Composites using Molecular Dynamics

*Prathamesh P. Deshpande, Matthew S. Radue, Prashik Gaikwad, Swapnil Bamane, Sagar Umesh Patil, William A. Pisani, Gregory M. Odegard**

Michigan Technological University, Houghton, MI-49931

Keywords

Computational Materials, Molecular Dynamics, Interface/interphase, High-performance polymer composites

Abstract

The next generation of ultra-high strength composites for structural components of vehicles for manned missions to deep space will likely incorporate flattened carbon nanotubes (flCNTs). With a wide range of

* Corresponding Author.

Email address: gmodegar@mtu.edu **(Gregory M. Odegard)**

high-performance polymers to choose from as the matrix component, efficient and accurate computational modeling can be used to efficiently down-select compatible resins, drive the design of these composites by predicting interface behavior, and provide critical physical insight into the flCNT/polymer interface. In this study, molecular dynamics simulation is used to predict the interaction energy, frictional sliding resistance, and mechanical binding of flCNT/polymer interfaces for epoxy, bismaleimide (BMI), and benzoxazine high-performance resins. The results indicate that the BMI has stronger interfacial interaction and transverse tension binding with flCNT interfaces, while the benzoxazine demonstrates the strongest levels of interfacial friction resistance. Comparison of these results with similar results from the literature for other high-performance resins indicates that BMI demonstrates the best overall compatibility with flCNTs for use in high-performance structural composites.

Introduction

The need for lightweight ultra-strong structural materials is increasingly being recognized for the next generation of space vehicles for deep-space human travel. To fulfill this need, significant focus has been placed on carbon nanotube (CNT) based composites materials [1-4]. These materials have the potential to exhibit superior thermo-mechanical properties relative to the current state-of-the-art composites [5, 6]. So far, a major shortcoming of these materials is their failure to translate these outstanding properties to higher length scales. Therefore, it is necessary to investigate and mitigate the failure of the CNT/matrix interfacial region to fully utilize the benefits of these materials.

A recent study by Downes et al. [7] introduced a novel fabrication method which generates stacks of flattened CNTs (flCNTs) resulting in self-aligned assemblages. These structures promote higher surface-to-surface contact which was evident when combined with a bismaleimide polymer matrix. The flCNT/BMI composite showed a twofold increase in tensile strength and a threefold increase in the tensile

modulus when compared to the round CNT composite counterpart [7]. Even though the flCNT-flCNT contact was enhanced by the flattening and stacking, the TEM-observed fracture surfaces showed intra-stack sliding in addition to complete stack pullout. A follow-up study by Jolowsky et al. [8] provided a pathway to scale the flCNT composite fabrication method to macro-scale panels with excellent mechanical properties. Patil et al. [9] reported the polymer/flCNT interfacial characteristics for two polyimide systems at the nanoscale using Molecular Dynamics (MD) techniques. It was reported that different chemical groups in the polymer had different effects on the polymer/flCNT interfacial interaction. Findings by Pisani et al. [10] affirmed the same by comparing PEEK and fluorinated and non-fluorinated cyanate esters.

Using MD, this study focuses on modelling the polymer/flCNT interface of three high-performance polymers: glycidylamine-based epoxy, bismaleimide (BMI), and poly-benzoxazine. All the simulated systems are aerospace-relevant thermosets [11-19] and each system is unique in terms of reaction chemistry and molecular topology. This study compliments the results published by Patil et al. [9] and Pisani et al. [10]. It is important to note that similar to Patil et al. [9] and Pisani et al. [10], experimental validation of the simulated results is not performed because fabrication and the relevant interfacial characterization methods for these materials have not yet been developed. This study is intended to drive the future development of such materials. The simulations discussed herein employ MD modelling techniques which have been previously experimentally validated [20-22].

Molecular Modeling

The details of the MD simulation are discussed in this section. The LAMMPS software package was used for all simulations discussed in this paper [23]. The Interface Force Field (IFF), developed by Heinz et al. [24], was designed to accurately model the properties of inorganic surfaces. Included in the original scope of IFF is the ability to capture inorganic-organic interfaces and the adsorption of organic molecules

onto inorganic surfaces. Recently, the Polymer Consistent Force Field was supplemented with IFF (PCFF-IFF) and proven successful for predicting the dispersibility of CNTs in different solvents and polymer solutions [25]. The PCFF-IFF forcefield was used to assign the interatomic potential in this study, as it was previously shown to yield accurate results for flCNTs and consists of all the relevant atom types associated with the amorphous polymer systems [9, 26]. Additionally, this force field can model the π electrons virtually which is critical to accurately capture the polymer-flCNT interface. The PCFF-IFF force field is well-known for its accurate atomic charge assignments, which has proven to have a significant effect on the predicted matrix-reinforcement interface characteristics and molecular conformations of polar molecules [9, 10].

Material Systems

The epoxy, BMI, and benzoxazine systems selected for this study consisted of the following monomers:

1. Epoxy: Tetraglycidyl methylenedianiline (TGMDA or TGDDM) and 4,4'-diaminodiphenyl sulfone (DDS) [27]
2. BMI: Bismaleimidodiphenylmethane (BMPM) and O,O'-diallyl bisphenol A (DABPA) [28]
3. Benzoxazine: Bisphenol-A benzoxazine [29]

High-performance polymer-based composite materials are extensively used in aerospace applications because of their excellent thermal and mechanical properties [2, 30]. These three polymer systems are thermosets that are specifically used for structural applications [12, 29, 31-35]. Molecular modeling studies exploring the thermo-mechanical properties have been previously performed on these specific polymers [27, 28, 36-39]. However, the influence of the molecular structure on the overall mechanical properties and reinforcement interface characteristics remains largely unexplored. Figure 1 shows the molecular structures of all the modelled monomers, and Figure 2 shows the equilibrated conformations.

1:1 molar ratios of BMPM to DABPA and TGMDA to DDS were used for the BMI and epoxy polymers, respectively [22, 27, 28, 36].

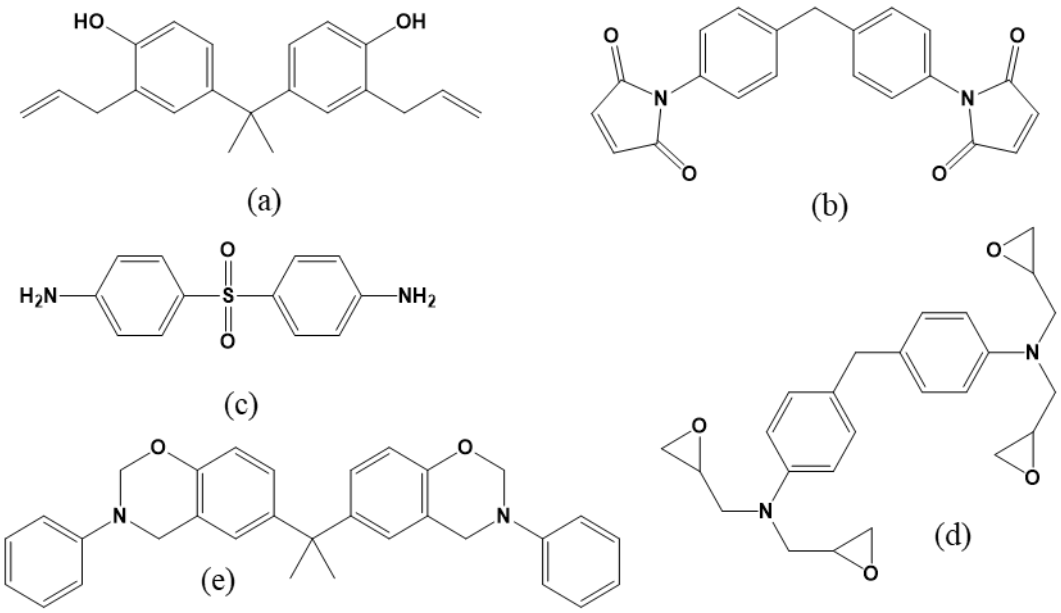

Figure 1. Chemical structures of (a) DABPA, (b) BMPM, (c) DDS, (d) TGMDA, and (e) Benzoxazine.

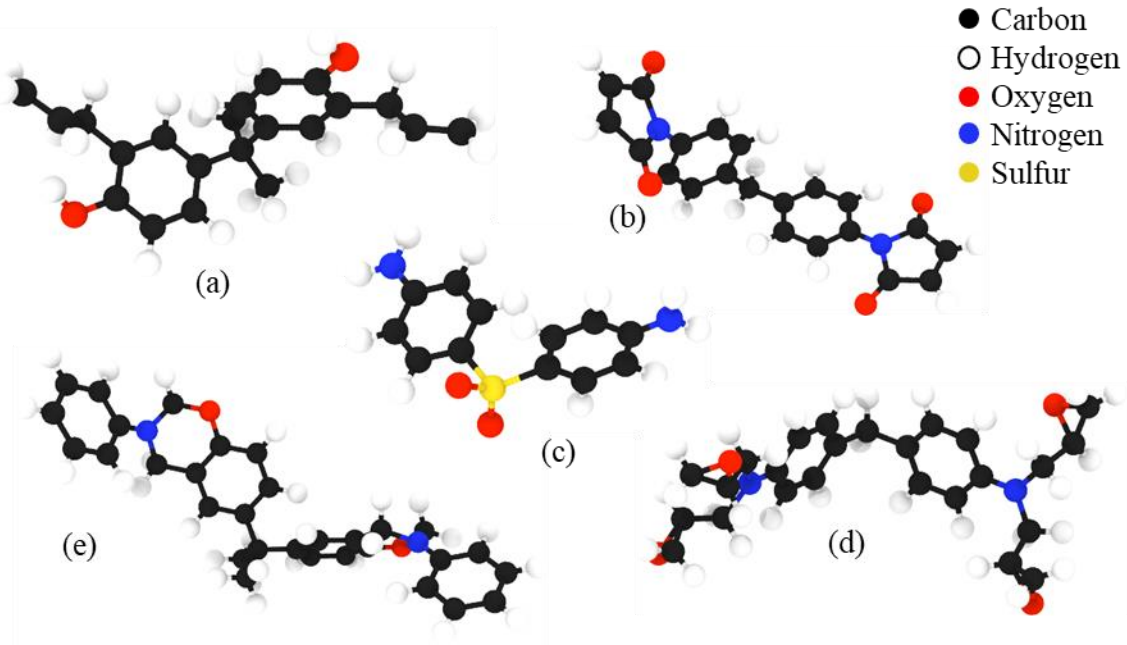

Figure 2. Molecular models of the monomeric units of (a) DABPA, (b) BMPM, (c) DDS, (d) TGMDA, and (e) Benzoxazine after molecular minimization in LAMMPS. OVITO was used for visualizations [40].

Model Setup

Figure 3 shows a representative MD model where the two flCNTs are modeled as two double-layered graphene surfaces, simply representing the flattened portion of the flCNTs. The rounded ends of the flCNTs shown in Figure 3(b) were excluded for computational efficiency [9, 10], as these features can be better captured with larger length scale models and this study is only focused on isolating the influence of the resin type on interfacial characteristics in the flattened region. In this work, previously established methodology has been adopted to model the three thermoset polymer composites using MD [9, 10]. All the simulation box boundaries are periodic, hence the polymer regions connected across the top and bottom of the Z boundary make up a single layer. This layered setup was chosen to represent the basic features of the sp^2 carbon flCNT-polymer interaction, friction, and transverse strength. While the model simulates the ideal scenario of complete polymer resin infiltration between flCNTs, the described setup is useful in extracting the critical interfacial features in the nanocomposite [41].

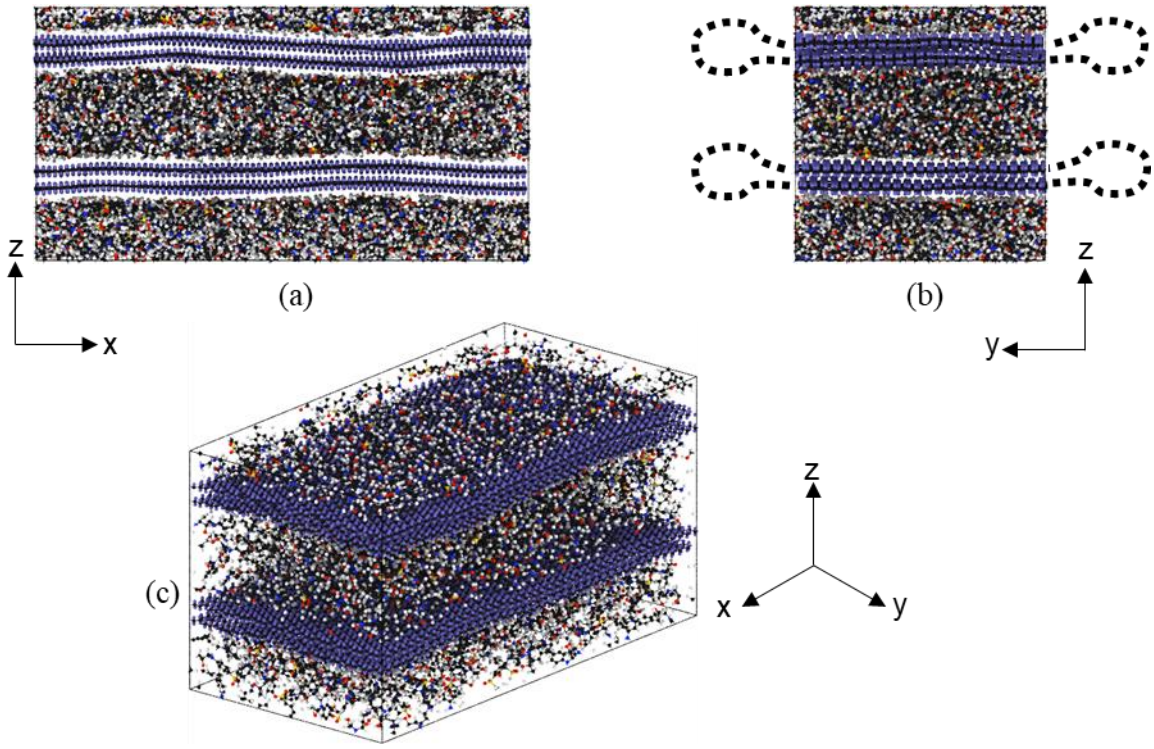

Figure 3. Representative model setup for the flCNT/epoxy composite (a) front view, (b) side view showing the side lobes of flCNTs, and (c) isometric view. The purple atoms attached to the flCNT carbon atoms represent the virtual π electrons.

The following steps demonstrate the workflow implemented in LAMMPS to build the MD models of flCNTs combined with BMI, epoxy, and benzoxazine for each polymer mass fraction. A 1 fs timestep and, the Nose-Hoover thermostat and barostat with "aniso" settings were used for all the simulations [42-45].

1. Relatively small simulation boxes were created to establish the equilibrium configuration of the stand-alone monomers, as shown in Figure 4(a). For the BMI, one DABPA monomer and one BMPM monomer were added to a simulation box (1:1 molar stoichiometry). For the epoxy, one TGMDA monomer and one DDS monomer were added to a simulation box (1:1 molar stoichiometry). For the benzoxazine, a single monomer was simulated in a simulation box. To

obtain the lowest energy configuration for each structure, a molecular minimization simulation was run by using the "minimize" command in LAMMPS using the conjugate gradient (CG) algorithm.

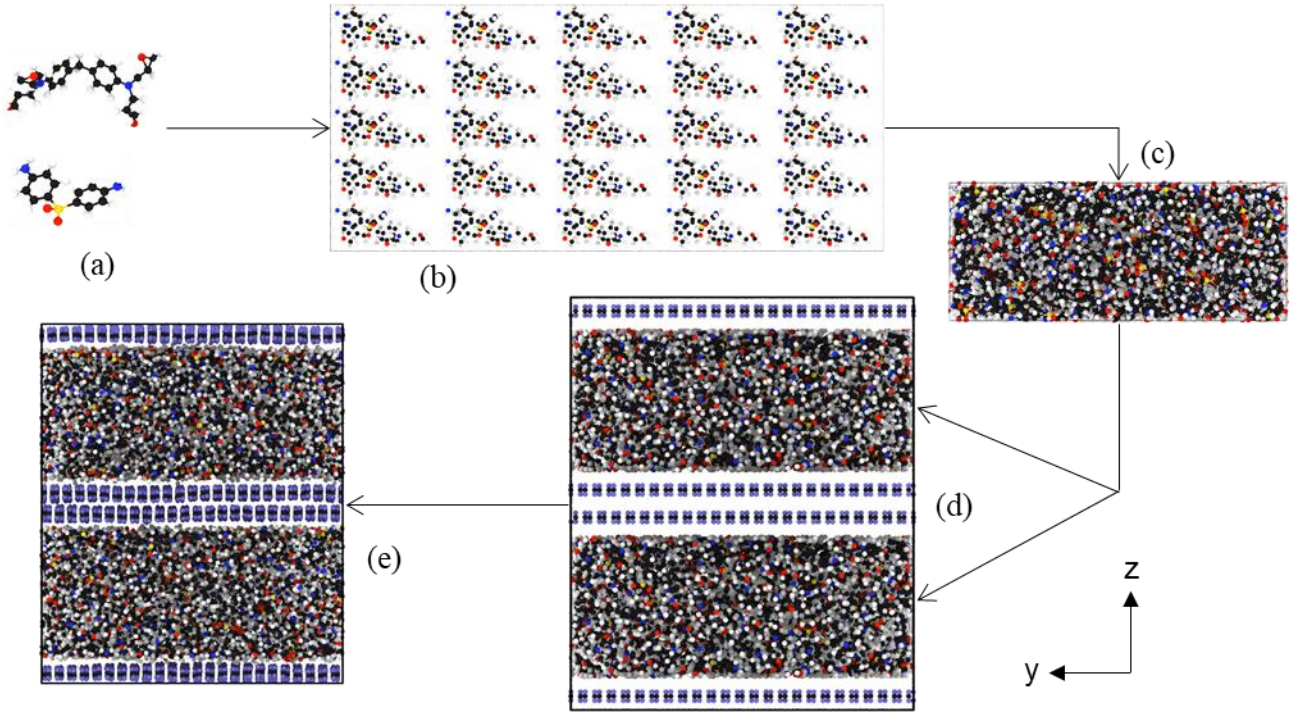

Figure 4. Molecular modelling workflow for the epoxy system: (a) Modeling individual monomers and placing them in a simulation box. (b) Replicating the box to form a bigger system. (c) Densifying the simulation box to closely pack the monomers. (d) Combine the compressed model with the flCNT. (e) Perform annealing, polymerization, and equilibration on the model to prepare for property prediction.

2. The monomer layer was first built without including the flCNTs. The equilibrated monomers from Step 1 were arranged in regularly-spaced arrays in a simulation box at a low initial mass density (approximately 0.1 g/cm^3) as shown in Figure 4(b). Molecular minimization simulations were run to ensure the monomers had their correct conformation before the next step.

3. The monomers were densified to target mass densities, shown in Table 1, for the BMI, epoxy, and benzoxazine resins [27, 28, 37, 38]. These density values were chosen as initial guesses, with the final mass densities achieved at the end of this step [21, 22, 46]. The X and Y dimensions of the simulation boxes were preset at 101 and 51 Å, respectively, since in a forthcoming step, fixed-dimension pseudo-flCNT layers were inserted [47]. The X and Y dimensions were kept constant for all the models to provide a uniform contact area at the interface. The densification simulations were performed at 300 K using the "fix deform" command in LAMMPS, where the Z dimension was gradually reduced at a constant rate as shown in Table 1. The box boundaries were non-periodic and reflecting in all three directions using the "fix wall/reflect" command in LAMMPS such that they could be effectively placed between flCNTs in the subsequent step [48]. The final densified layer is shown in Figure 4(c).
4. For assembling the layered MD models, a periodic box of 101×51 Å dimensions in the X-Y plane was created. The single densified monomer layer from Step 3 was duplicated in the Z direction, creating a second identical layer. The second layer was necessary to run the friction simulations described below. The two layers were separated by 10 Å in the Z direction and 5 Å of empty space was added on top and bottom of the polymer layers to accommodate the two flCNTs. Because the boundaries were periodic, the polymer layer was now allowed to traverse the boundary. The flCNT layers with 23,616 atoms each were inserted into the free spaces to complete the setup as shown in Figure 4(d). This method of combining the monomer layers and flCNTs helped to maintain the flatness of the flCNTs. Upon assembly, the model was relaxed using an energy minimization. These layer models were developed to achieve a series of specific overall monomer mass fractions. The mass fraction, in this case, is the ratio of molecular mass of monomers to the molecular mass of the entire system including the flCNTs. In this work,

individual models for mass fractions ranging from 10 % to 80 % were built for the three polymer systems with sizes ranging from 25,000 – 65,000 atoms.

Table 1. MD modeling details for the model-building simulations.

	BMI	Epoxy	Benzoxazine
Polymer layer densification			
Target density (g/cm3)	1.20	1.29	1.20
Densification rate (Å/ns)	10	10	10
Annealing			
Annealing temperatures (K)	750 - 300	600 - 300	600-300
cooling rate (K/ns)	75	50	50
Polymerization			
Run time (ns)	2	0.5	2
Temperature	650	400	650
Reaction probability (step1)	0.00001	0.0001	0.01
Reaction probability (step2)	--	0.01	0.1
Reaction probability (step3)	--	--	0.99
Reaction probability (step4)	--	--	0.99
Bond cutoff distance (Å)	6	6	7
Final Equilibration			
Run time (ns)	2	2	2

5. The assembled layered MD models were equilibrated by running a 100 ps simulation using the NPT ensemble with the temperature and pressure set to 300 K and 1 atm, respectively. Next, the system temperature was increased above the glass transition temperature of each polymer system and annealed for 100 ps using the NPT ensemble. Finally, the model was cooled back down to

300 K over 6 ns with a constant cooling rate. The simulation details are provided in Table 1. To allow the simulation box volume to adjust for the changes in temperature, a Nose-Hoover barostat was set to maintain a pressure of 1 atm.

6. After annealing, the models were virtually cured by performing polymerization simulations. Polymerization simulations were performed using the REACTER protocol as demonstrated by Gissinger et al. [49]. Rather than using in-house scripts, this choice provides a highly reproducible procedure for crosslinking polymers [49, 50]. The simulation settings are listed in Table 1. All the polymerization simulations were performed using 1 fs timesteps in the NVT ensemble. The precise details of the polymerization steps for the three polymers are provided in the Supporting Information, Section S1. Figure 5 shows the maximum conversions for all the models.

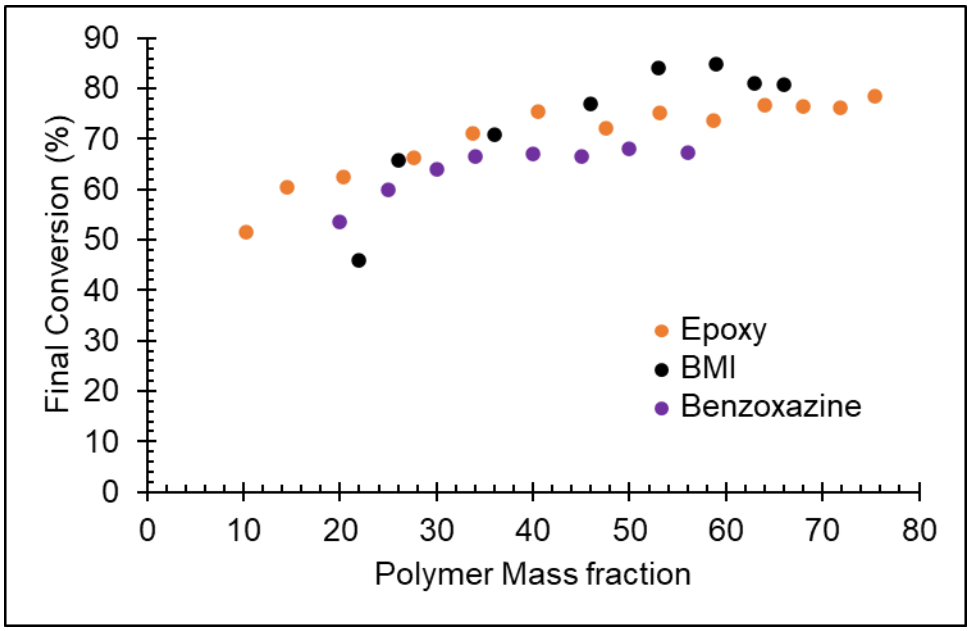

Figure 5. Maximum conversion achieved in the three systems based on polymer concentration.

7. After polymerization, the models were annealed, again, using identical settings as described in Step 5. This second stage of annealing was performed to help the new networks find more

desirable configurations [51]. After annealing, the models were equilibrated to prepare for room temperature property prediction. Table 1 lists the equilibration simulation settings.

Figure 6 shows the atomic mass densities along Z-direction and highlights the higher atomic densities near the interface for all the models. The higher polymer density at the interface can be seen in the form of a secondary peak (red-dotted circles) adjacent to the larger peaks, which represent flCNT atoms. Figure 7, Figure 8, and Figure 9 show the polymerized models for different polymer mass fractions. Within these figures, the left-most image displays the lowest polymer mass fraction resulting in clustering of polymer atoms. The middle image displays a perfectly saturated interface with the two flCNT layers completely separated by the polymer atoms. The right-most image displays the highest polymer mass fraction which results in addition of excessive polymer atoms. Detailed polymer mass fractions and the respective molecular masses are included in the Supporting Information, Section S2.

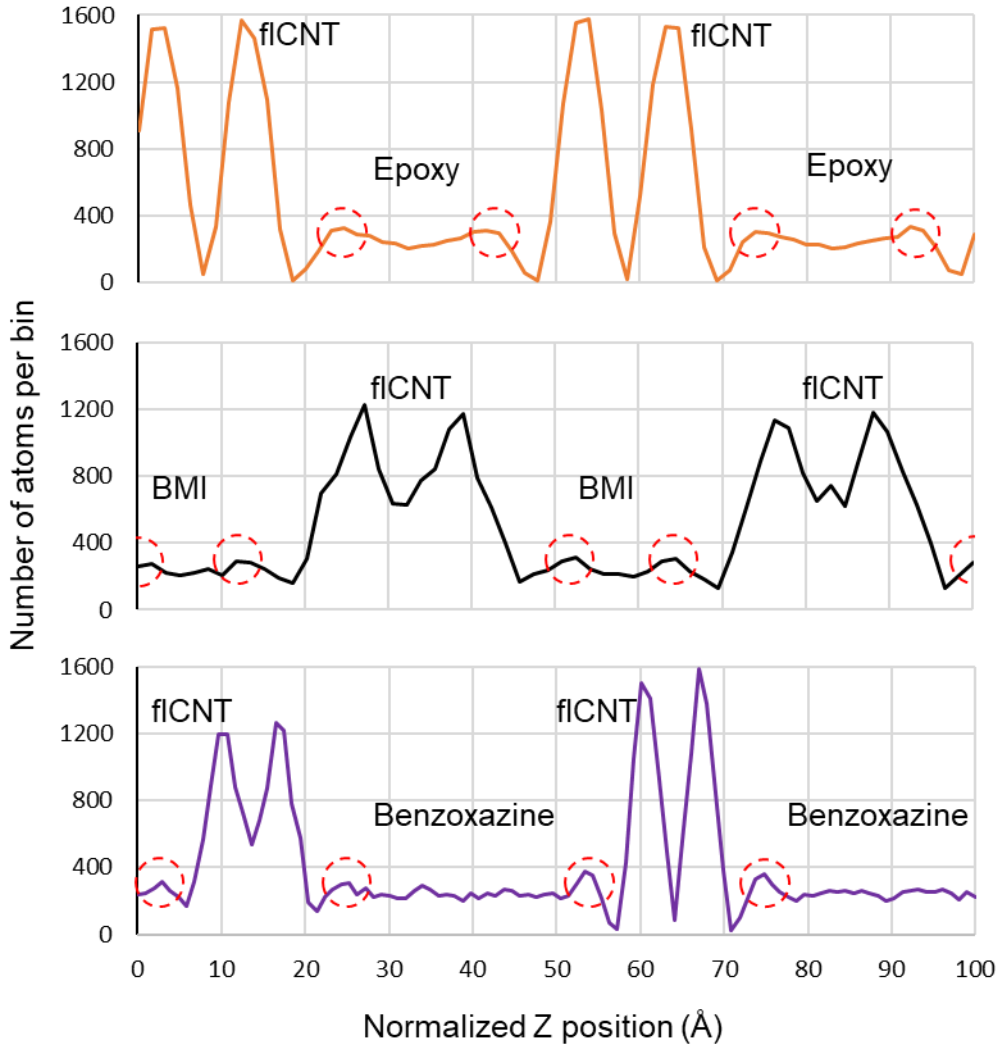

Figure 6. Atomic count profile for the three systems (40.52% Epoxy, 45.84% BMI, and 40% Benzoxazine) showing the distribution for 0.5 Å bin size. Secondary peaks (red-dotted circle) highlighting the interfacial saturation by polymer atoms.

The equilibrated models were then evaluated for the interfacial interaction energy, friction resistance, and transverse strength. The interaction energy and friction simulations were also carried out on unpolymerized models to assess the effect of polymerization. To compute the interaction energy, the purely non-bonded potential energy unrelated to the polymer and flCNTs was extracted from the model using the help of the "compute group/group" command in LAMMPS [52, 53]. For all models, the

simulations were performed in the NPT ensemble over 0.5 ns to collect the time-averaged interaction energy data. Temperature and pressure settings of 300 K and 1 atm respectively were used for all of these simulations.

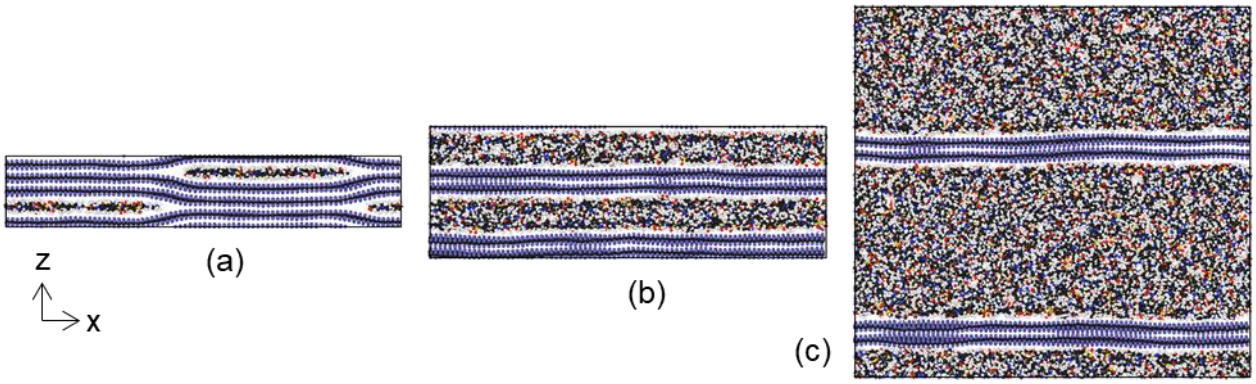

Figure 7. Molecular models of flCNT/ epoxy composite with mass fraction, from left (a) 10% (b) 41% (c) 75%.

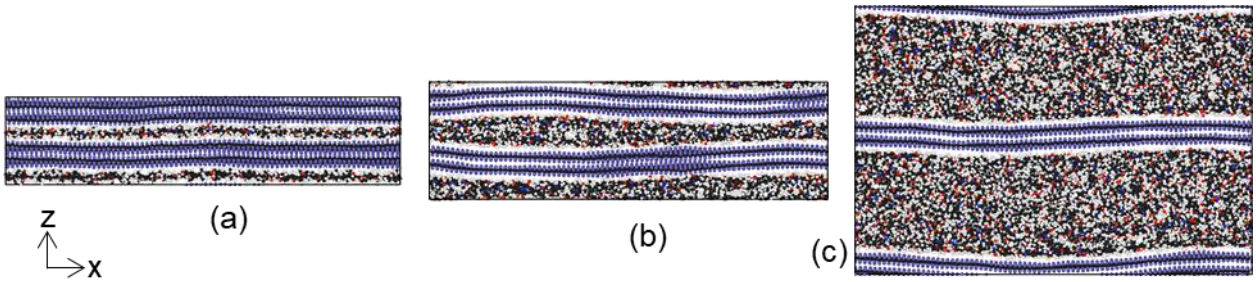

Figure 8. Molecular models of flCNT/BMI composite with mass fraction, from left (a) 22% (b) 36% (c) 66%.

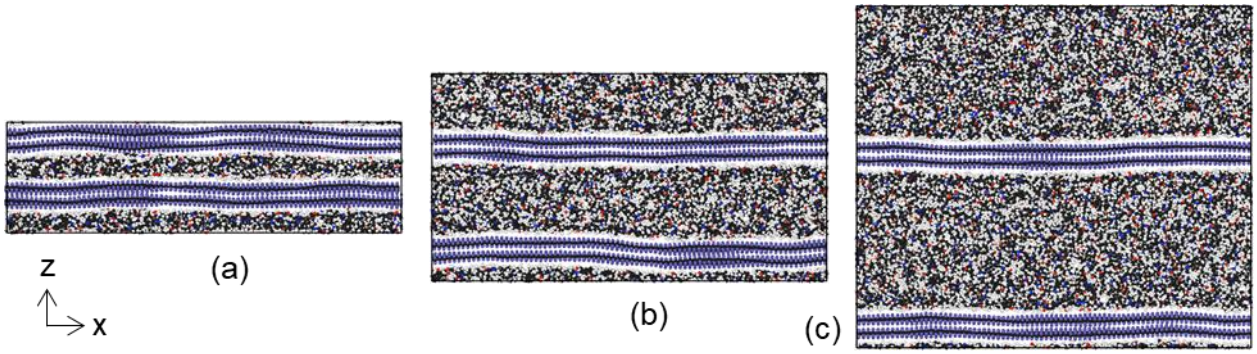

Figure 9. Molecular models of flCNT/ benzoxazine composite with mass fraction, from left (a) 20% (b) 34% (c) 56%.

Patil et al. [9] demonstrated a novel approach to compute atomistic friction force between polymer-infiltrated flCNTs using the same simulation geometry described herein. Using the same approach, friction simulations were performed on both the unpolymerized and polymerized models for each resin system. For all the models, both the flCNTs were tethered to two distinct points with a virtual spring using LAMMPS. The spring constant used for both the springs was set to 1 kcal/mol·Å^2. The point connected to the bottom layer was linearly displaced in the X direction using a velocity range of 0.1 Å/ps to 5 Å/ps. The other layer was held in position using the NPT ensemble with 300 K temperature and 1 atm pressure. The polymer layers and the sliding flCNT were maintained under the NVE ensemble, allowing the temperature to change, and thus enhancing the vibrations at the interfaces. The resulting friction force was computed between the moving flCNT and the polymer layer, and the fixed flCNT and the polymer layer.

The third criterion studied is the transverse strength of the layered models. The equilibrated models of the three polymer systems with a polymer mass fraction of approximately 0.4 were used for this evaluation. This polymer mass fraction is comparable with previously reported data [9, 10]. To assess the transverse tension behavior, the simulation box was subjected to a uniaxial strain in the direction perpendicular to the flCNT plane at a constant strain rate of 2×10^8 s^{-1} until there was total separation of

one of the CNT/polymer interfaces or a maximum of 150% strain was reached. The overall system stresses and strains were recorded, and the corresponding stiffness, strength, and toughness values were calculated [9]. An R script was used for this analysis.

Results

Interaction energy

The interaction energy for the unpolymerized and polymerized models of the three resins are shown in Figure 10. The displayed trendlines are to distinguish multiple datasets and provide clear trends amongst the scattered data points. It is important to note that the trendlines do not bear any physical significance. The interaction energy values carry a negative sign which indicates attraction to the aromatic surface of the flCNT. Therefore, higher negative values indicate greater polymer/surface affinity. Figure 10 shows dramatic increases in interaction energy for all the three systems, both monomer and polymer, with increases in polymer mass fraction, except for the polymerized benzoxazine system.

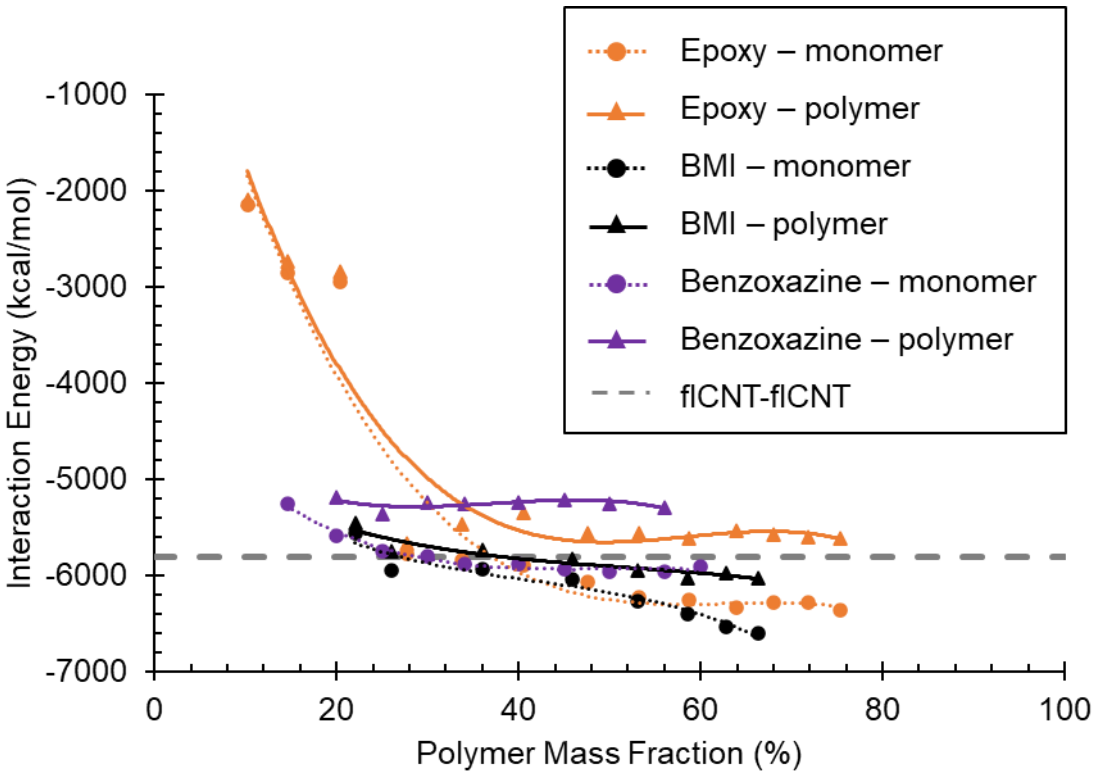

Figure 10. Interaction energy between flCNTs and polymer layers with varying polymer mass fraction for monomer and polymer cases.

For the epoxy system, the data in Figure 10 indicates the strengthening of interaction depends highly on the effective saturation of the polymer-flCNT interface. The initial increase is significant and is due to clustering of polymer molecules at the interface for lower mass fractions, which is evident from Figure 7. Well-distributed monomers are observed in the interfacial region at polymer mass fractions 33% or greater. For higher polymer mass fractions, the flCNTs were completely encompassed by a 10 Å or thicker polymer region, and the interaction energy stays relatively constant.

The data in Figure 10 indicates that the BMI models did not exhibit the same initial steep trend with the interaction energy as observed with the epoxy. However, unlike the epoxy, increases in the interaction energy were observed with increases in the mass fraction over the entire range of mass fractions. This

behavior is attributed to the preferential adsorption of the BMPM molecules. The molecular models in this study indicate that BMPM binds better with flCNT than DABPA, which is exemplified in Figure 11. In Figure 11, the largest flCNT/BMI monomer model, with a monomer mass fraction of 0.66, was divided into equal-width (about 0.7 Å) slices along the Z-direction. The flCNT, BMPM, and DABPA atoms in each slice were counted separately to reveal the molecular spatial variation. The flCNT appears as two sets of double spikes. Note that some waviness in the flCNT caused the peaks to broaden in comparison with perfectly straight layers [46]. The BMPM and DABPA spatial distributions are strikingly contrasting. Immediately flanking the flCNTs are high concentrations of BMPM, but in the same region, the DABPA atoms are depleted. Moving further away from the flCNT layers, the concentration of DABPA increases and becomes more prominent. Essentially, Figure 11 reveals partial monomer separation: the BMPM monomers move toward the flCNT, while the DABPA monomers tend to be driven away from the flCNT. Section S3 from the supporting information provides a more qualitative analysis on BMPM planarization. The epoxy, also a two-part system, did not develop preferential adsorption of either of its components.

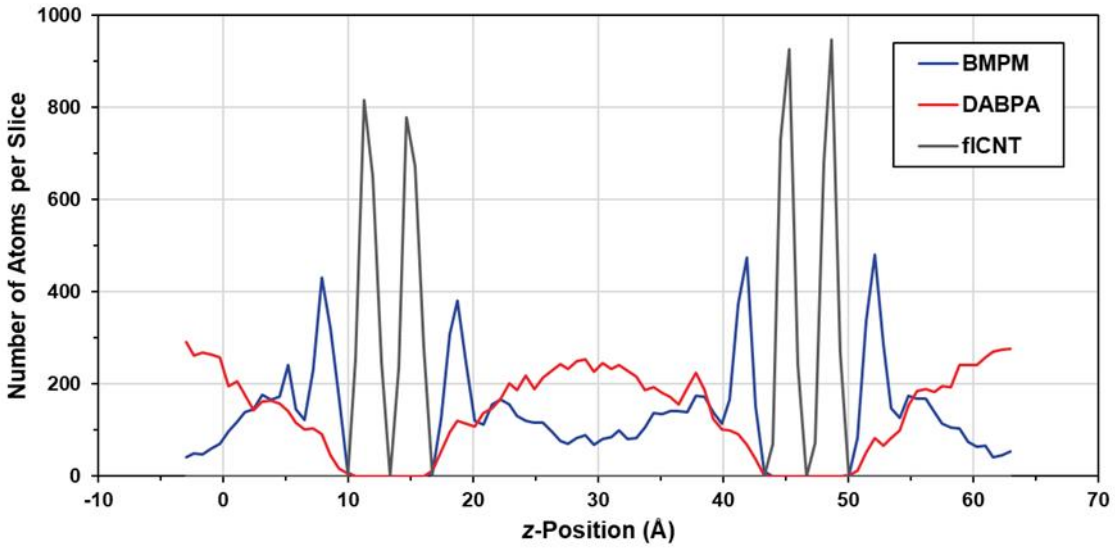

Figure 11. Atomic count profile demonstrating preferential adsorption of BMPM monomer. The atoms were binned by their z-position with bin sizes of about 0.7 Å, and for each bin, the number of atoms were counted.

From Figure 10, increasing the polymer mass fraction has very little to no effect on the interaction energy of the benzoxazine system. At 34% polymer mass fraction the interaction energy trend converges and remains approximately the same for higher mass fractions. This observation can be explained by Figure 9, where the lowest mass fraction model displayed perfect separation of the two flCNT layers. Hence, the interface was completely populated by the polymer atoms for all the mass fractions.

Post-polymerization, the interaction energy plots shift upwards indicating loss of interaction strength due to the new networked polymer topology. For benzoxazine, the effect of polymerization on the interaction energy is significant, however, saturation of the interface for the polymerized system has no effect on the interaction energy. In the case of epoxy and BMI, the interaction energy shifts slightly but maintains the same trend as observed with the unpolymerized models. With BMI, preferential adsorption of BMPM is still present but less impactful. Figure 12 shows the orientation of the phenyl rings in the monomer and polymer structures with respect to the flCNT surface. It is well-documented that phenyl

groups promote aromatic-aromatic non-bonded stacking, a.k.a. π-π stacking [54-57]. The orientations were computed by extracting the dihedral angles of the phenyl rings within the polymer layers. The angle was calculated with respect to the X-Y plane of the flCNT surface, ignoring deviations caused due to slight waviness as seen in Figure 7-Figure 9. Lower angles represent greater degrees of alignment with the flCNT surface. The monomer/polymer mass fractions used for this analysis correspond to the converged interaction energies, specifically, BMI: 58.52%, Epoxy: 58.66%, and Benzoxazine: 56%. This analysis was conducted to provide physical insight into the interaction energy trends. Earlier studies have shown the non-bonded interactions between the aromatic groups is a strong contributor towards the interaction energy [57].

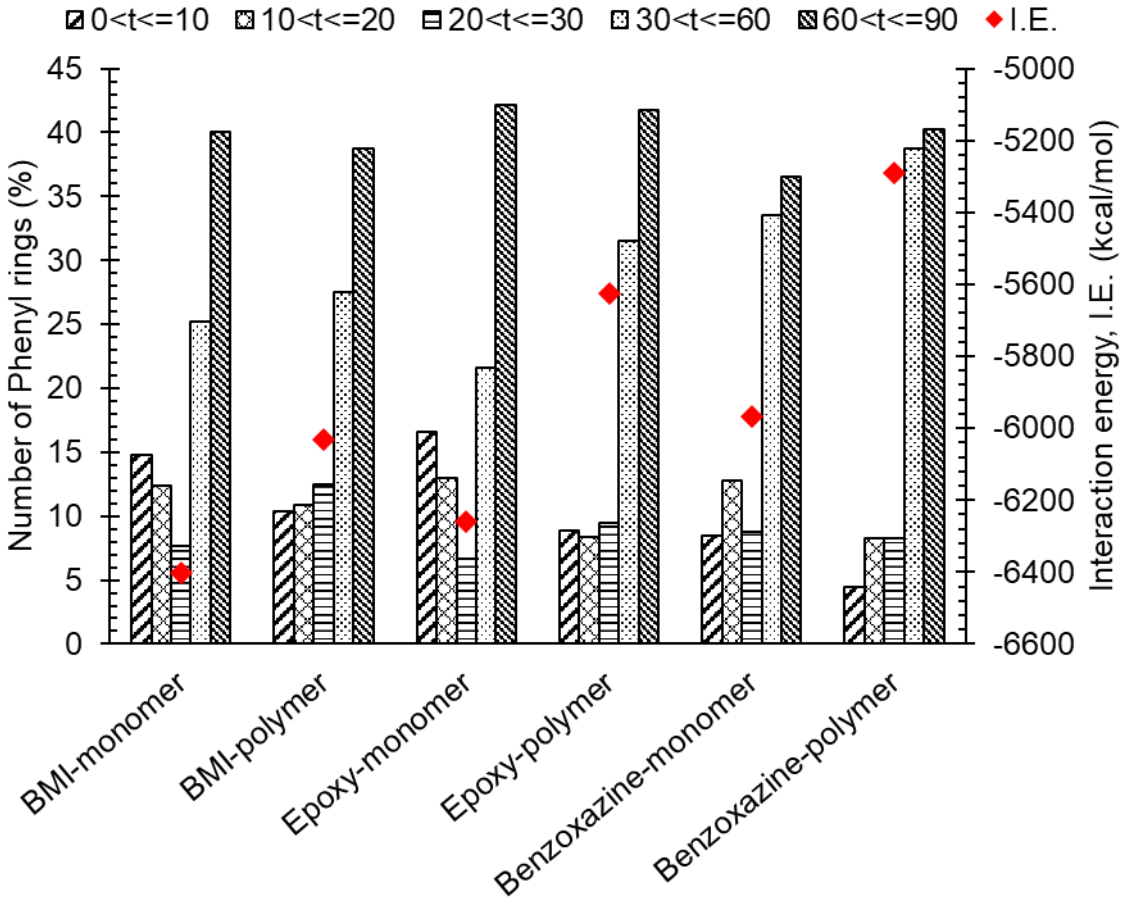

Figure 12. Alignment of phenyl rings (dihedral angles) and interaction energies for BMI, epoxy, and benzoxazine, t (degrees) is dihedral angle formed by the phenyl rings with the XY plane.

Figure 12 clearly shows the decrease in interfacial interaction when the monomers undergo polymerization and result in lower numbers of phenyl rings aligned with the interface. The creation of networks results in additional mobility constraints which results in higher angles between the phenyl rings and the flat aromatic surface. Within each polymer system, the number of phenyl rings with less than 10^{o} angle is reduced after crosslinking. All three resins systems demonstrate similar patterns in interaction energy and polymerization, however, the preferential adsorption in BMI helps in limiting the reduction in interaction energy after polymerization, which is highlighted in Figure 112. The epoxy models show a higher drop in the interaction energy since neither of the two components strongly prefer the flCNT

surface. Figure 13 shows the number of phenyl rings with a dihedral angle of less than or equal to 10° with the flCNT surface for the BMI and epoxy systems highlighting the orientations from the individual components. It can be concluded that the BMI models benefit greatly with the increasing mass fractions at the expense of adding mass to the system. Benzoxazine shows poor alignment of the phenyl rings with the surface due to the rigid backbone of the monomer.

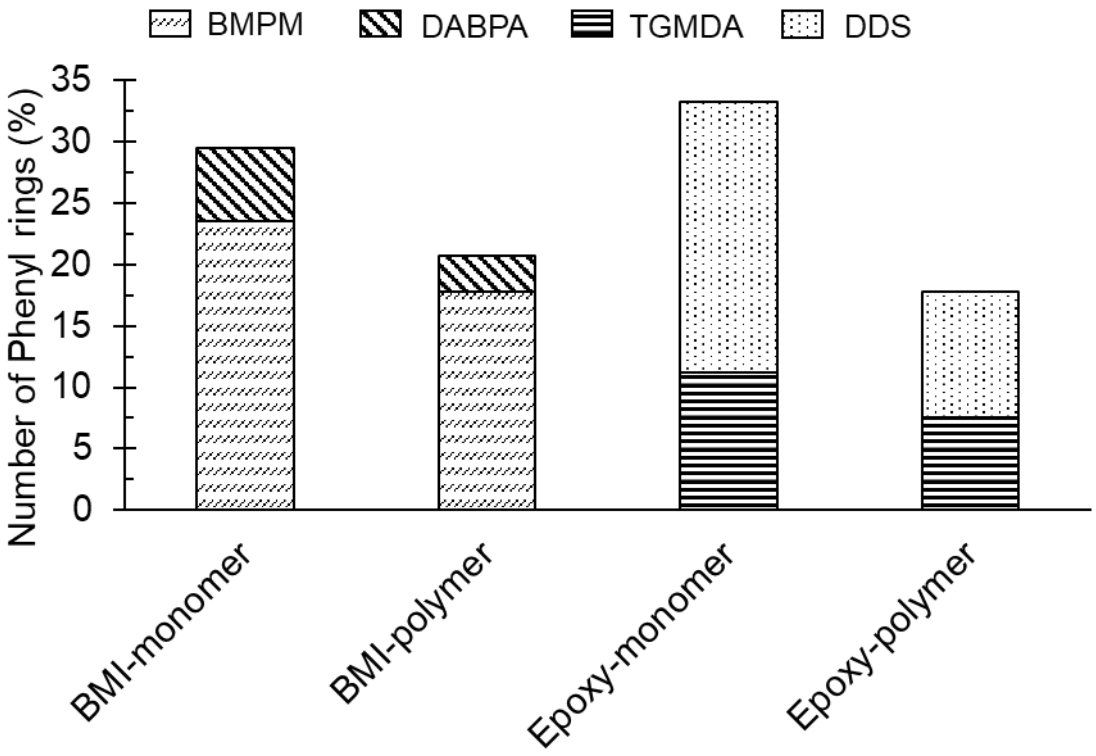

Figure 13. Alignment of phenyl rings with a dihedral angle of 10° or less for the individual components of the BMI and epoxy systems.

Figure 14 shows the interaction energy for multiple polymer systems including those reported in previous studies [9, 10]. The previously studied polymer systems were all single-component systems. The PEEK and non-fluorinated polyimide show the highest degree of interaction, whereas the fluorinated polymers have a relatively low level of interaction because of steric hindrance from the fluorinated groups.

The interaction from the benzoxazine is also relatively low. The interaction energy of BMI and epoxy systems lie in the middle of the other polymers. BMI shows slightly better affinity due to the preferential adsorption of BMPM molecules. BMI is the only thermoset in this group with an interaction energy that is lower than that of the bare flCNTs.

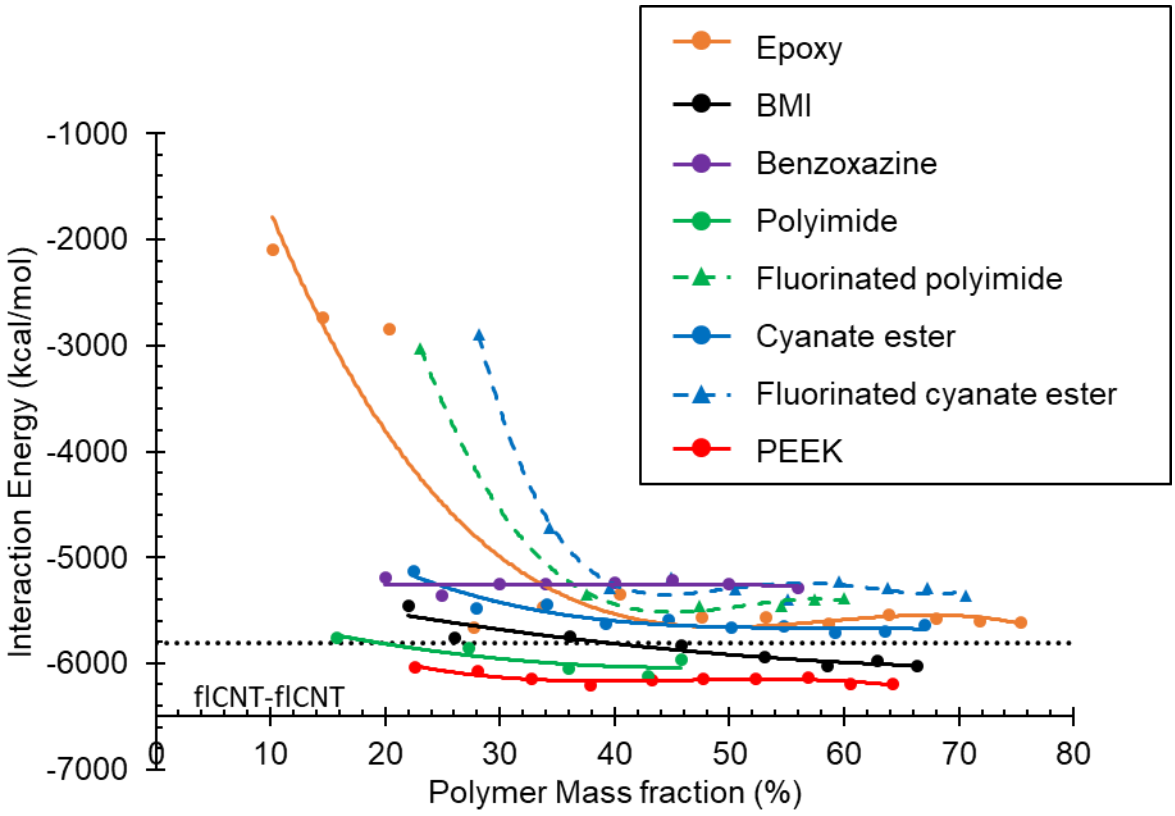

Figure 14. Interaction energy between flCNTs and polymer layers with varying polymer mass fraction for a wide range of polymers, including data from Pisani et al. [10] and Patil et al. [9].

Frictional Resistance

The results from the friction simulations are detailed in this section for both the monomers and polymers. The trend lines used in all the figures are included to visually distinguish between the datasets and do not hold any physical significance.

Figure 15 reveals the friction force trend for the polymerized and unpolymerized models of all three polymer systems, as well as the friction force associated with flCNTs with no polymer (commensurate and incommensurate). The incommensurate flCNT-flCNT friction case is considered to accurately represent the actual stacking configuration in flCNT stacks [58, 59]. As reported previously, the presence of a polymer layer results in an increase of two orders of magnitude in the friction force exhibited by the incommensurate flCNT-flCNT [9, 10]. Models with polymer mass fractions of 64% in epoxy, 66% in BMI, and 56% in benzoxazine are used for this comparison. At low velocities, the three polymers (both monomeric and polymeric forms) display a close performance because of the scarcity of polymer atoms at the interface. Benzoxazine displays superior resistance when simulating both low and high velocities. Crosslinking of the model significantly enhances the friction force for BMI and epoxy, but not for the Benzoxazine over most of the range of velocities. The effect of polymerization for these three systems displays an inverse trend as seen from the interaction energy study, where polymerization reduced the interaction, yet increases the frictional force. Polymerization imposes additional restrictions on the movement of the monomeric units by the formation of a polymer network. The formation of a more rigid network causes a greater amount of coarsening (i.e. protrusion of constrained molecular groups into the flCNT surface) and thus increased interface friction, whereas un-crosslinked monomers can more easily conform to the flCNT surface and thus form a smoother interface with less friction. Figures S6 and S7 display the minimum and maximum polymer mass fraction models for the three systems for the unpolymerized and polymerized conditions, respectively.

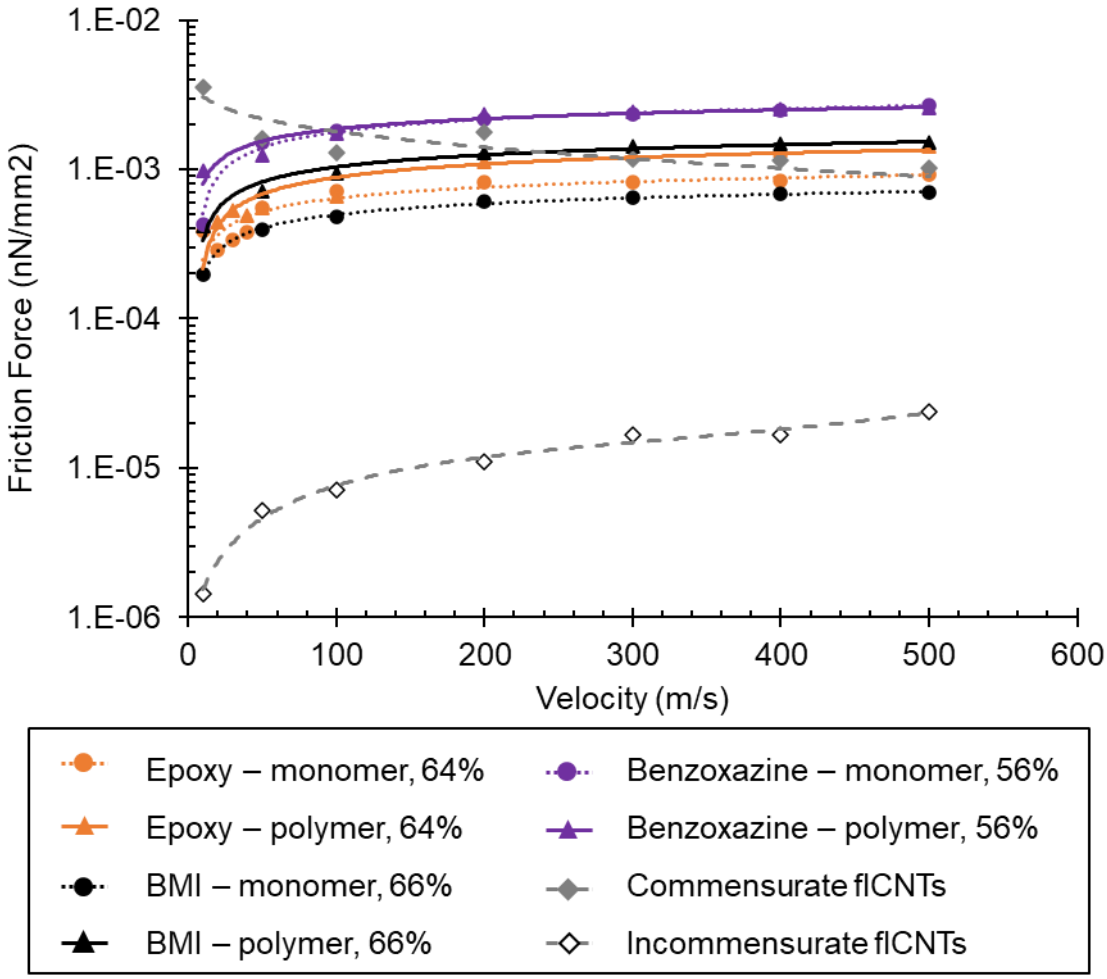

Figure 15. Friction force of the polymer systems and commensurate/incommensurate flCNTs as a function of velocity for monomer and polymer cases.

In Figure 16, the effect of polymer mass fraction on the frictional resistance is demonstrated for the entire collection of flCNT-polymer models and no discernable trend was observed for the range of mass fractions. The results from 10 m/s sliding velocity were chosen for comparison. For all the models, the friction force increases post-polymerization. As seen in Figure 10, the observations indicate an inverse relation between the friction force and interaction energy. That is, polymers exhibiting higher interaction energies exhibited lower frictional resistance, and the systems with lower interaction energy generally displayed better friction force. Also, polymerization degrades the interaction energy of all the polymers,

however, it enhances the friction force for the same systems. Figure S5 from the supporting information shows the data for other velocities and similar trends were observed.

To summarize the results for the friction simulations, Figure 17 shows the frictional force curves of the polymerized models and includes results for the polyimide, PEEK, and cyanate ester systems from Patil et al. [9] and Pisani et al. [10]. The benzoxazine system shows higher frictional resistance in comparison to the fluorinated polymers. It was reported that the fluorinated polymers exhibit higher friction due to the presence of the trifluoromethyl groups [9]. The epoxy and BMI systems also exhibit a good frictional resistance amongst the non-fluorinated polymers. Figure S4 is the supporting information shows the comparison of the same polymers for different polymer mass fractions with a 10 m/s velocity, and like Figure 16, no discernable trend was observed.

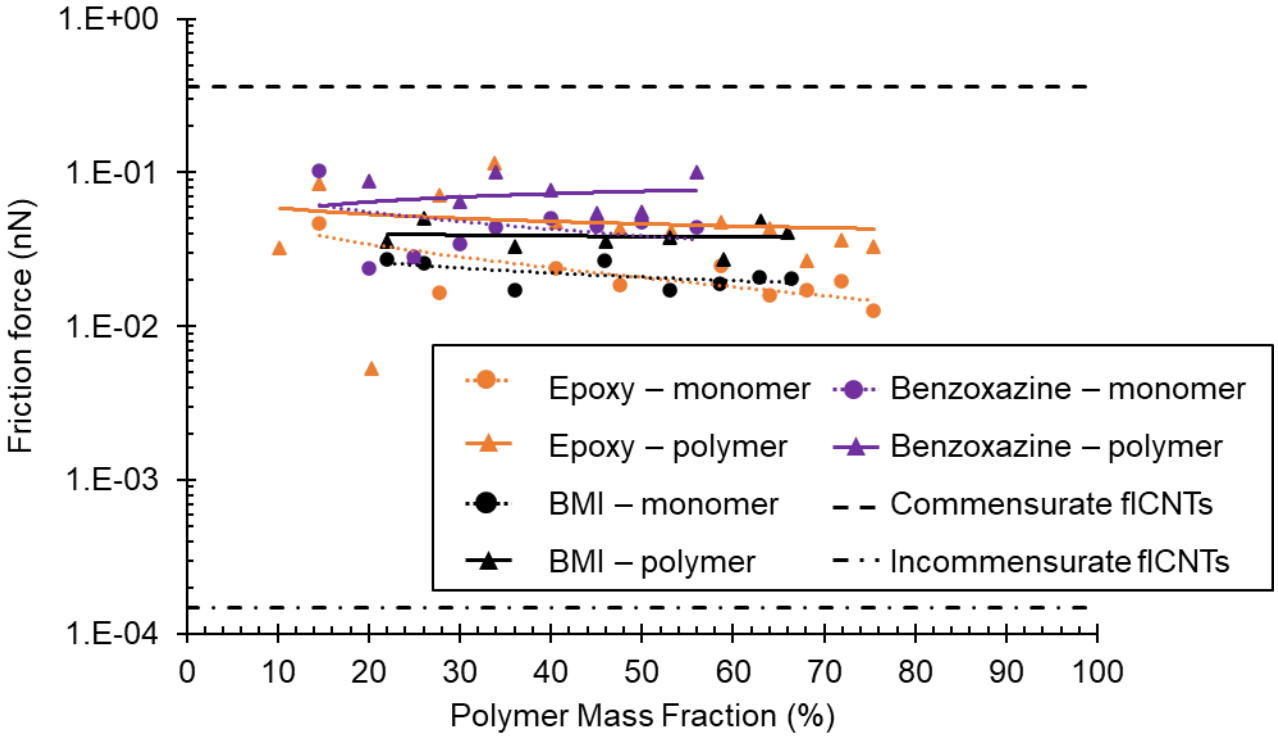

Figure 16. Friction force as a function of polymer mass fraction at a velocity of 10 m/s for monomer and polymer cases, and commensurate/incommensurate flCNTs.

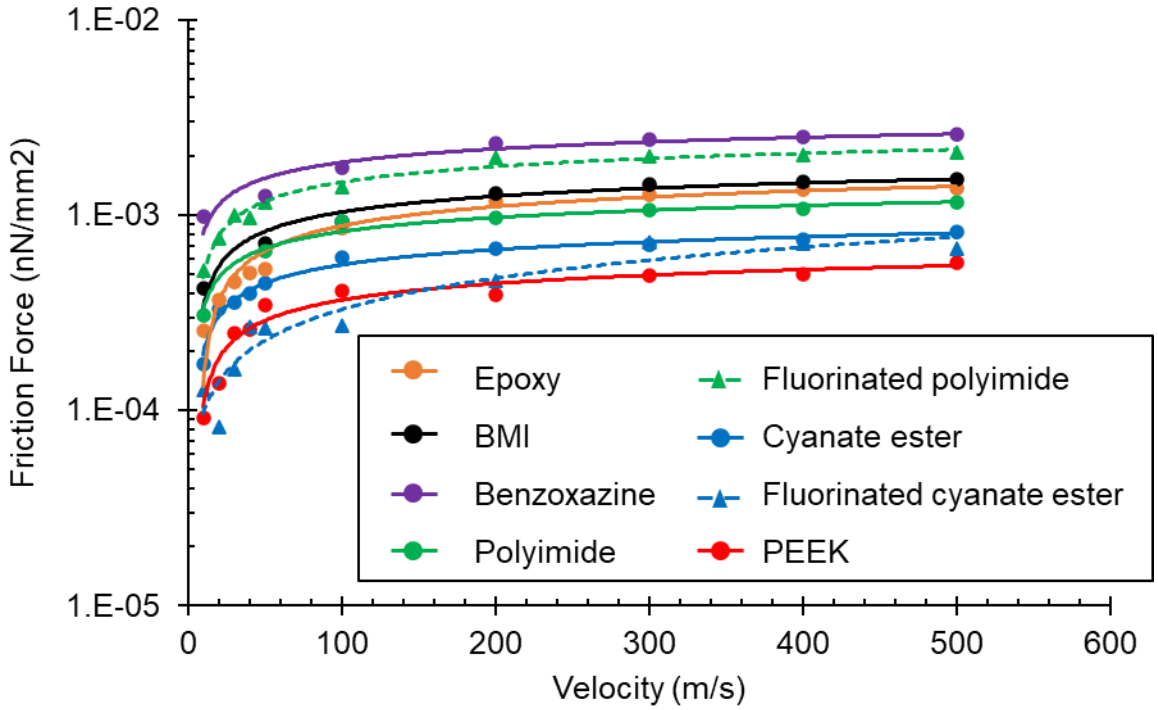

Figure 17. Friction force of polymer systems as a function of velocity for the polymer case, including data from Pisani et al. [10] and Patil et al. [9].

Transverse Strength

Figure 18 shows the stress-strain response from the transverse tension simulations for polymer mass fractions of 41% for epoxy, 36% for BMI, and 34% for benzoxazine. The selection of these polymer mass fractions was based on those of other polymer systems reported in previous work [9, 10]. From the figure, the epoxy and the BMI models exhibit a higher peak strength than the benzoxazine. However, the benzoxazine system displays a higher toughness which is evident from the corresponding curve not converging to the 0 MPa stress value. Figure 19 shows snapshots of the three models either at the end of simulation or when one of the polymer layers completely separated.

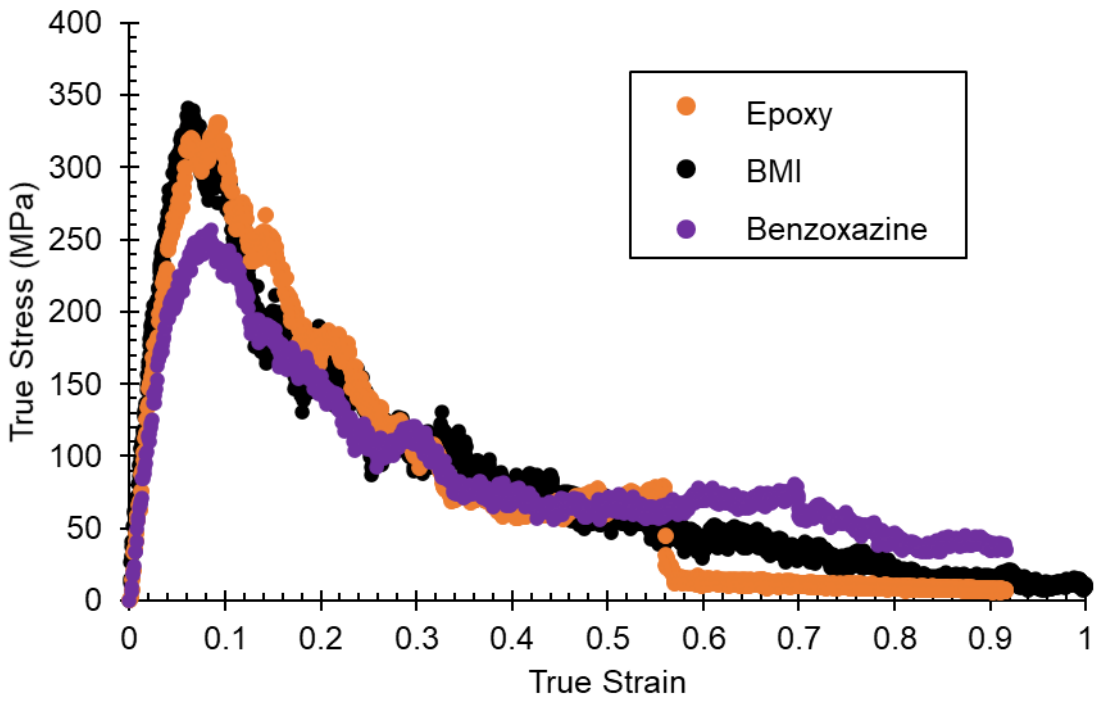

Figure 18. Stress-strain curves of the three polymerized systems in transverse tension.

Figure 20 includes the transverse tension results for all the polymer systems including the corresponding data for the polyimide, cyanate ester, and PEEK systems from previous studies [9, 10]. The stiffness, toughness, and peak strength values are normalized with respect to the results obtained from a neat flCNT-flCNT transverse tension simulation. From the comparison, BMI shows the best performance in all the three metrics. Epoxy shows the second highest stiffness and peak strength but lower toughness than benzoxazine and the fluorinated cyanate ester. From Figure 19, it is clear that separation of the polymer layer occurs much earlier in the epoxy system relative to the BMI and benzoxazine systems, resulting in the lower overall toughness.

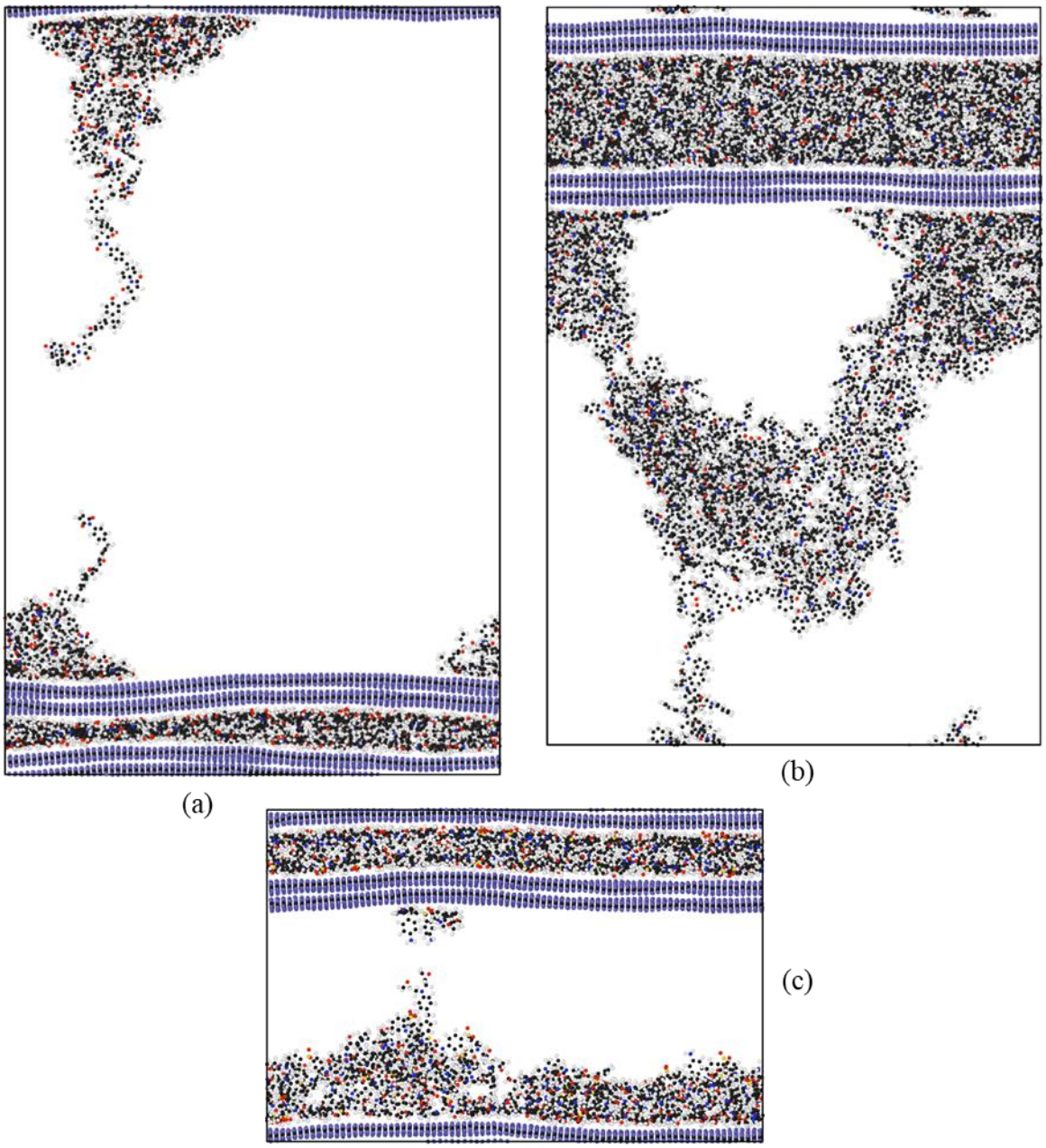

Figure 19. Snapshot of final separation of the (a) BMI, (b) benzoxazine, and (c) epoxy with the flCNTs when subjected to transverse tension.

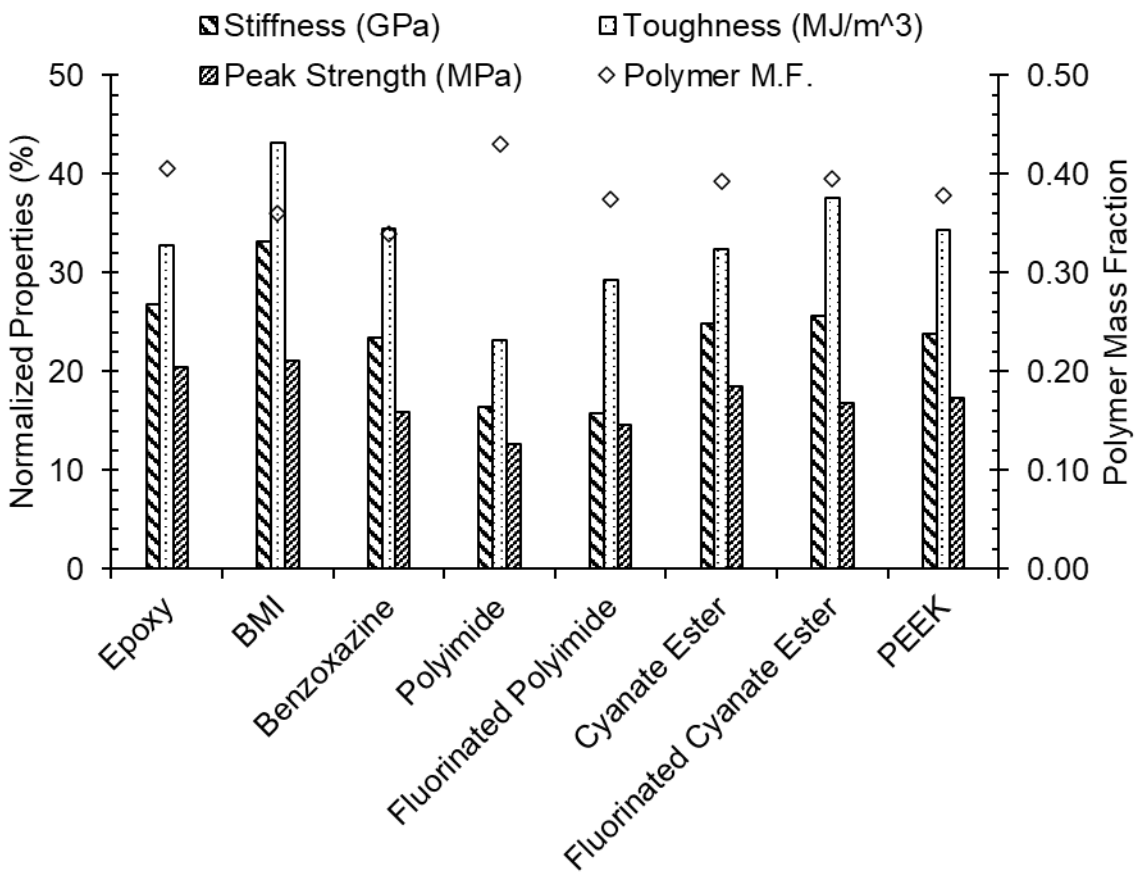

Figure 20. Normalized stiffness, toughness, and peak strength, and the corresponding polymer mass fraction for the polymerized polymer/flCNTs.

Conclusion

The PCFF-IFF forcefield was used for MD simulations of three high-performance thermoset polymers and flCNT systems with various levels of polymer layer thicknesses. Specifically, tetrafunctional epoxy, BMI, and benzoxazine resins were studied to investigate their interfacial compatibility with the flCNT surface. BMI and epoxy produced similar interaction energies with BMI showing greater interaction with the flCNT surface than flCNTs show with each other. In particular, the BMPM monomer was shown to preferentially adsorb onto the flCNT surface. This resulted in monomer separation within the BMI layers. Furthermore, the thicker BMI monomer layers produced a relatively strong interaction energy due to the

high number of preferred BMPM monomers which could migrate toward the interface. The interaction energies of the BMI and epoxy systems were 14% and 6.29% higher than that of the benzoxazine system, respectively.

From the dynamic friction simulations, the presence of polymer layers demonstrated dramatic enhancement of the frictional force over that of the bare incommensurate flCNTs. Results strongly suggest that the presence of the polymer layer, regardless of the concentration, improves the friction at the interfaces. Benzoxazine outperformed BMI and epoxy by 41% and 42% respectively. The transverse tension simulations conducted on the three systems reported three metrics: stiffness, toughness, and peak strength. BMI produces the best results for all the three metrics.

Summarizing the results, BMI produces the best overall compatibility with the flCNTs with the epoxy showing a similar trend but with a slight under-performance. Including the previously reported systems, PEEK still shows the best interaction with the flCNTs with the polyimide and BMI also showing higher interaction than bare flCNTs [9, 10]. However, benzoxazine exhibits a much superior friction force than the other two systems in this study and the two fluorinated systems from Patil et al. [9] and Pisani et al. [10]. With a best performance in two out of the three metrics, including the three sub-metrics from transverse tension, the BMI appears to be the polymer matrix of choice when considering the flCNT stacks. However, in the design of such nanocomposites, careful consideration may be required in balancing the three described metrics as per the application. Therefore, the molecular insights gained from this research can be helpful in guiding the selection of resin systems for the engineering of new flCNT-based composites.

Supporting Information

The following document is available free of charge. The document (PDF) includes details on the polymerization for the three resin systems, configuration of all the nanocomposite models, qualitative analysis on BMPM planarization and additional details on the frictional resistance results.

Acknowledgements

This research was supported by the NASA Space Technology Research Institute (STRI) for Ultra-Strong Composites by Computational Design (US-COMP), grant NNX17AJ32G. SUPERIOR, a high-performance computing cluster at Michigan Technological University, was used in obtaining the MD simulation results presented in this publication.

References

1. NASA, *2020 NASA Technology Taxonomy*. 2020, NASA.

2. Kim, J.-W., et al., *Assessment of carbon nanotube yarns as reinforcement for composite overwrapped pressure vessels.* Composites Part A: Applied Science and Manufacturing, 2016. **84**: p. 256-265.

3. Kim, J.-W., et al., *Modifying carbon nanotube fibers: A study relating apparent interfacial shear strength and failure mode.* Carbon, 2021. **173**: p. 857-869.

4. Bellucci, S., et al., *CNT composites for aerospace applications.* Journal of Experimental Nanoscience, 2007. **2**(3): p. 193-206.

5. Baur, J. and E. Silverman, *Challenges and Opportunities in Multifunctional Nanocomposite Structures for Aerospace Applications.* MRS Bulletin, 2007. **32**(4): p. 328-334.

6. Siochi, E.J. and J.S. Harrison, *Structural nanocomposites for aerospace applications.* MRS Bulletin, 2015. **40**(10): p. 829-835.

7. Downes, R.D., et al., *Geometrically constrained self-assembly and crystal packing of flattened and aligned carbon nanotubes.* Carbon, 2015. **93**: p. 953-966.

8. Jolowsky, C., et al., *Microstructure evolution and self-assembling of CNT networks during mechanical stretching and mechanical properties of highly aligned CNT composites.* Composites Science and Technology, 2018. **166**: p. 125-130.

9. Patil, S.U., et al., *Interfacial characteristics between flattened CNT stacks and polyimides: A molecular dynamics study.* Computational Materials Science, 2020. **185**.

10. Pisani, W.A., et al., *Interfacial modeling of flattened CNT composites with cyanate ester and PEEK polymers.* Composites Part B: Engineering, 2021. **211**.

11. Song, Y., et al., *Carbon nanotube sensor thread for distributed strain and damage monitoring on IM7/977-3 composites.* Smart Materials and Structures, 2014. **23**(7).

12. Kaiser, A.L., I.V. Albelo, and B.L. Wardle, *Fabrication of Aerospace-grade Epoxy and Bismaleimide Matrix Nanocomposites with High Density Aligned Carbon Nanotube Reinforcement*, in *AIAA Scitech 2020 Forum*. 2020, American Institute of Aeronautics and Astronautics.

13. Liu, Y., et al., *Shape memory polymers and their composites in aerospace applications: a review.* Smart Materials and Structures, 2014. **23**(2).

14. Adrian Lowe, B.F., Vincent Otieno-Alego, *Interfacial ageing of high temperature carbon/bismaleimide composites.* Composites Science and Technology, 2002. **33**(10): p. 1289-1292.

15. Gu, A., et al., *Bismaleimide/carbon nanotube hybrids for potential aerospace application: I. Static and dynamic mechanical properties.* Polymers for Advanced Technologies, 2007. **18**(10): p. 835-840.

16. Kirmani, M.H., et al., *Cure Behavior Changes and Compression of Carbon Nanotubes in Aerospace Grade Bismaleimide-Carbon Nanotube Sheet Nanocomposites.* ACS Applied Nano Materials, 2021.

17. Hatsuo Ishida, T.A., *Handbook of Benzoxazine Resins*. 2011: Elsevier.

18. Comer, A.J., et al., *OOA (Out-of-Autoclave) manufacturing of benzoxazine resin-systems by lri (liquid-resin-infusion) for ambient and high temperature aerospace applications*. 2014.

19. Barile, C., C. Casavola, and F. De Cillis, *Mechanical comparison of new composite materials for aerospace applications.* Composites Part B: Engineering, 2019. **162**: p. 122-128.

20. Bandyopadhyay, A., et al., *Molecular modeling of crosslinked epoxy polymers: The effect of crosslink density on thermomechanical properties.* Polymer, 2011. **52**(11): p. 2445-2452.

21. Pisani, W.A., et al., *Multiscale modeling of PEEK using reactive molecular dynamics modeling and micromechanics.* Polymer, 2019. **163**: p. 96-105.

22. Radue, M.S., et al., *Comparing the Mechanical Response of Di-, Tri-, and Tetra-functional Resin Epoxies with Reactive Molecular Dynamics.* J Polym Sci B Polym Phys, 2018. **56**(3): p. 255-264.

23. Plimpton, S., *Fast Parallel Algorithms for Short-Range Molecular Dynamics.* Journal of Computational Physics, 1995. **117**: p. 1-19.

24. Heinz, H., et al., *Thermodynamically consistent force fields for the assembly of inorganic, organic, and biological nanostructures: the INTERFACE force field.* Langmuir, 2013. **29**(6): p. 1754-65.

25. Pramanik, C., et al., *Carbon Nanotube Dispersion in Solvents and Polymer Solutions: Mechanisms, Assembly, and Preferences.* ACS Nano, 2017. **11**(12): p. 12805-12816.

26. Dharmawardhana, C.C., et al., *Reliable computational design of biological-inorganic materials to the large nanometer scale using Interface-FF.* Molecular Simulation, 2017. **43**(13-16): p. 1394-1405.

27. Hundley, J.M., et al., *Multi-Scale Modeling of Metal-Composite Interfaces in Titanium-Graphite Fiber Metal Laminates Part I: Molecular Scale.* Open Journal of Composite Materials, 2011. **01**(01): p. 19-37.

28. Radue, M.S., et al., *Molecular Modeling of Cross-Linked Polymers with Complex Cure Pathways: A Case Study of Bismaleimide Resins.* Macromolecules, 2018. **51**(5): p. 1830-1840.

29. ALLEN, H.I.a.D.J., *Physical and Mechanical Characterization of Near-Zero Shrinkage Polybenzoxazines.* Journal of Polymer Science: Part B: Polymer Physics, 1996. **34**: p. 1019-1030.

30. Zhe Liu, Y.-S.D., Matthew Lundblad, Ayou Hao and Zhiyong Liang, Youssef Aider and Yeqing Wang, *Lightweight and Flexible Thermal Protection Systems for High Temperature Composite Applications*, in *SAMPE 2020*. 2020: Virtual Series.

31. Cheng, Q., et al., *High Mechanical Performance Composite Conductor: Multi-Walled Carbon Nanotube Sheet/Bismaleimide Nanocomposites.* Advanced Functional Materials, 2009. **19**(20): p. 3219-3225.

32. Cheng, Q., et al., *Functionalized carbon-nanotube sheet/bismaleimide nanocomposites: mechanical and electrical performance beyond carbon-fiber composites.* Small, 2010. **6**(6): p. 763-7.

33. Sandi G. Miller, J.K.S., Daniel A. Scheiman, Michael Maryanski, and Michelle Schlea, *STUDY OF OUT-TIME ON THE PROCESSING AND PROPERTIES OF IM7/977-3 COMPOSITES*, in *SAMPE 2010*. 2010: Seattle, WA.

34. Vincent J.Lopata, C.B.S., Ajit Singh, Christopher J.Janke, George E.Wrenn, Stephen J.Havens, *Electron-beam-curable epoxy resins for the manufacture of high-performance composites.* Radiation Physics and Chemistry, 1999. **56**(4): p. 405-415.

35. Ishida, Y.-X.W.a.H., *Synthesis and Properties of New Thermoplastic Polymers from Substituted 3,4-Dihydro-2H-1,3-benzoxazines.* Macromolecules, 2000. **33**(8): p. 2839-2847.

36. Okabe, T., et al., *Curing reaction of epoxy resin composed of mixed base resin and curing agent: Experiments and molecular simulation.* Polymer, 2013. **54**(17): p. 4660-4668.

37. Saiev, S., et al., *Modeling the formation and thermomechanical properties of polybenzoxazine thermosets.* Polymer Chemistry, 2017. **8**(38): p. 5988-5999.

38. Thompson, S., et al., *Exploring Structure(-)Property Relationships in Aromatic Polybenzoxazines Through Molecular Simulation.* Polymers (Basel), 2018. **10**(11).

39. Won-KookKim, W.L.M., *A fully atomisticmodel of an amorphous polybenzoxazine at bulk density.* Computational and Theoretical Polymer Science, 1998. **8**: p. 353-361.

40. Stukowski, A., *Visualization and analysis of atomistic simulation data with OVITO–the Open Visualization Tool.* Modelling and Simulation in Materials Science and Engineering, 2009. **18**(1): p. 015012.

41. Damirchi, B., et al., *ReaxFF Reactive Force Field Study of Polymerization of a Polymer Matrix in a Carbon Nanotube-Composite System.* The Journal of Physical Chemistry C, 2020. **124**(37): p. 20488-20497.

42. Martyna, G.J., D.J. Tobias, and M.L. Klein, *Constant pressure molecular dynamics algorithms.* The Journal of Chemical Physics, 1994. **101**(5): p. 4177-4189.

43. Tuckerman, M.E., et al., *A Liouville-operator derived measure-preserving integrator for molecular dynamics simulations in the isothermal–isobaric ensemble.* Journal of Physics A: Mathematical and General, 2006. **39**(19): p. 5629-5651.

44. M. Parrinello, A.R., *Polymorphic transitions in single crystals: A new molecular dynamics method.* J Appl Phys, 1981. **52**(12): p. 7182-7190.

45. Shinoda, W., M. Shiga, and M. Mikami, *Rapid estimation of elastic constants by molecular dynamics simulation under constant stress.* Physical Review B, 2004. **69**(13).

46. Al Mahmud, H., et al., *Multiscale modeling of carbon fiber- graphene nanoplatelet-epoxy hybrid composites using a reactive force field.* Composites Part B: Engineering, 2019. **172**: p. 628-635.

47. Maoshuai He, J.D., Kaili Zhang, Feng Ding, Hua Jiang, Annick Loiseau, Juha Lehtonen, and Esko I. Kauppinen, *Precise Determination ofthe Threshold Diameter for a Single-Walled Carbon Nanotube To Collapse.* ACS Nano, 2014. **8**(9): p. 9657-9663.

48. Bond, S.D. and B.J. Leimkuhler, *Stabilized Integration of Hamiltonian Systems with Hard-Sphere Inequality Constraints.* SIAM Journal on Scientific Computing, 2008. **30**(1): p. 134-147.

49. Gissinger, J.R., B.D. Jensen, and K.E. Wise, *REACTER: A Heuristic Method for Reactive Molecular Dynamics.* Macromolecules, 2020. **53**(22): p. 9953-9961.

50. Gissinger, J.R., B.D. Jensen, and K.E. Wise, *Chemical Reactions in Classical Molecular Dynamics.* Polymer (Guildf), 2017. **128**: p. 211-217.

51. Huber, T., A.E. Torda, and W.F. van Gunsteren, *Local elevation: A method for improving the searching properties of molecular dynamics simulation.* Journal of Computer-Aided Molecular Design, 1994. **8**(6): p. 695-708.

52. Bogusz, S., T.E. Cheatham, and B.R. Brooks, *Removal of pressure and free energy artifacts in charged periodic systems via net charge corrections to the Ewald potential.* The Journal of Chemical Physics, 1998. **108**(17): p. 7070-7084.

53. Radue, M., *Molecular Modeling of Aerospace Polymer Matrices Including Carbon Nanotube-Enhanced Epoxy*, in *Mechanical Engineering-Engineering Mechanics*. 2017, Michigan Technological University. p. 126.

54. Huber, R.G., et al., *Heteroaromatic pi-stacking energy landscapes.* J Chem Inf Model, 2014. **54**(5): p. 1371-9.

55. McGaughey, G.B., M. Gagne, and A.K. Rappe, *pi-Stacking interactions. Alive and well in proteins.* J Biol Chem, 1998. **273**(25): p. 15458-63.

56. Mutasem Omar Sinnokrot, E.F.V., and C. David Sherrill, *Estimates of the Ab Initio Limit for π−π Interactions: The Benzene Dimer.* J. Am. Chem. Soc., 2002. **124**(36): p. 10887-10893.

57. Mingjun Yang, V.K., and Michael Zaiser, *Interactions between Polymers and Carbon Nanotubes: A Molecular Dynamics Study.* J. Phys. Chem. B, 2005. **109**(20): p. 10009-10014.

58. Xu, H., J. Al-Ghalith, and T. Dumitrică, *Smooth sliding and superlubricity in the nanofriction of collapsed carbon nanotubes.* Carbon, 2018. **134**: p. 531-535.

59. Xu, H., et al., *Collapsed carbon nanotubes: From nano to mesoscale via density functional theory-based tight-binding objective molecular modeling.* Carbon, 2019. **143**: p. 786-792.